BIOCHEMISTRY
including biophysical chemistry & molecular biology

ARTICLE

pubs.acs.org/biochemistry

Deep-UV Resonance Raman Analysis of the *Rhodobacter capsulatus* Cytochrome bc_1 Complex Reveals a Potential Marker for the Transmembrane Peptide Backbone

Christopher M. Halsey, Olayinka O. Oshokoya, Renee D. Jiji, and Jason W. Cooley*

Department of Chemistry, University of Missouri, Columbia, Missouri 65211, United States

S *Supporting Information*

ABSTRACT: Classical strategies for structure analysis of proteins interacting with a lipid phase typically correlate ensemble secondary structure content measurements with changes in the spectroscopic responses of localized aromatic residues or reporter molecules to map regional solvent environments. Deep-UV resonance Raman (DUVRR) spectroscopy probes the vibrational modes of the peptide backbone itself, is very sensitive to the ensemble secondary structures of a protein, and has been shown to be sensitive to the extent of solvent interaction with the peptide backbone [Wang, Y., Purrello, R., Georgiou, S., and Spiro, T. G. (1991) J. Am. Chem. Soc. 113, 6368−6377]. Here we show that a large detergent solubilized membrane protein, the *Rhodobacter capsulatus* cytochrome bc_1 complex, has a distinct DUVRR spectrum versus that of an aqueous soluble protein with similar overall secondary structure content. Cross-section calculations of the amide vibrational modes indicate that the peptide backbone carbonyl stretching modes differ dramatically between these two proteins. Deuterium exchange experiments probing solvent accessibility confirm that the contribution of the backbone vibrational mode differences are derived from the lipid solubilized or transmembrane α-helical portion of the protein complex. These findings indicate that DUVRR is sensitive to both the hydration status of a protein's peptide backbone, regardless of primary sequence, and its secondary structure content. Therefore, DUVRR may be capable of simultaneously measuring protein dynamics and relative water/lipid solvation of the protein.

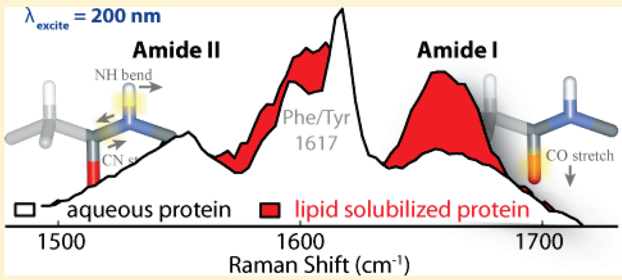

Transmembrane (TM) proteins play a role in nearly every facet of cellular homeostasis, yet at the structural level, they remain the least understood class of proteins.[1] Despite well-documented difficulties in purifying and crystallizing TM proteins, as well as issues associated with molecular size, detailed structural resolution has been obtained through X-ray crystallography or NMR for proteins that protein can be crystallized or are not too large.[2] Structural information may potentially come from yet to be realized variants of these techniques, i.e., small-angle X-ray scattering,[3] or from newly emerging techniques such as neutron scattering.[4,5] More facile and established techniques can give gross or ensemble secondary structure resolution, such as infrared absorption[6] or circular dichroism spectroscopies.[7,8] However, these techniques fail in addressing structural fluctuations in membrane proteins as they cannot easily differentiate between membrane embedded and solvent accessible portions of a protein without significant sample modification. Fluorescence or electron paramagnetic resonance analyses using aromatic residues,[9] or fluorescent[10,11] or paramagnetic probes chemically attached to proteins, have proven particularly useful for locating a region of a protein in relation to the membrane lipid phase as well as giving information about the transient environment that such residues experience kinetically.

Deep-UV (λ_{ex} < 210 nm) excited resonance Raman (DUVRR) spectroscopy has proven to be a useful tool for elucidating secondary structural content and its changes in soluble proteins.[12−14] DUVRR has the advantage that various structurally constrained protein regions (those with differing secondary structures) have differing spectral intensities due to variable excitation cross sections. Additionally, since the intensity of signal relies on the polarizability of the bonding orbitals in the excited versus the ground state, electron-withdrawing processes, such as hydrogen bonding from solvent, will have a significant impact on the intensity of any or all of the amide I (C=O stretch), II and III (out-of-phase or in-phase N−H bending/C−N stretching, respectively), or S (coupled N−H/C_α−H bending) modes.[15−18] Furthermore, since the target of investigation is the peptide backbone, which is inherent to all protein sequences, the protein sequence need not be modified in most cases. For these reasons and its amenability to a variety of measurement time scales, DUVRR has proven to be a useful tool for the structural analysis of protein samples that would be commonly classified as problematic for structural analysis, i.e., those that are insoluble or highly dynamic on the measurement scale. In fact, time-resolved events of

Received: April 19, 2011
Revised: June 27, 2011
Published: June 30, 2011

cooperative allostery in globins, basic tenets of protein unfolding, and secondary structure formation and characterization of different secondary structure domains within large protein aggregates have all been resolved by DUVRR analyses.[19] DUVRR has also proven to be sensitive enough to delineate the structure and dynamics of discrete subdomains even within very short homo-polypeptides.[20]

Recently, standard, or non-deep-UV excited ($\lambda_{ex} > 220$ nm), resonance Raman, sensitive to the aromatic vibrational modes of a protein, has been employed to analyze membrane protein catalytic events in photosystems,[21,22] protein folding, and insertion of pore complexes and dynamics of inter-TM strand hydrogen bonding within a membrane interior.[23] However, examination of the structure of membrane-associated proteins has not been realized by DUVRR, presumably due to presuppositions about the complexity of the samples. Specifically, the presence of superstoichiometric lipid or detergent molecules and the presence of various cofactors could potentially interfere with spectral quality and interpretability by contributing spectral features of their own to the resonance Raman spectra or by absorbing enough incident light to disallow adequate scattering from the protein backbone to allow for DUVRR spectral collection.

The cytochrome (cyt) bc_1 complex from *Rhodobacter capsulatus* (Rcaps) is a good model for testing the feasibility of the analysis of membrane protein structure and solvation by DUVRR, as it can be purified with good yield from Rcaps[24] and is well characterized for its function as well as its detailed atomic structure.[25−28] Specifically, the cyt bc_1 complex satisfies several sample related potential spectroscopic pitfalls associated with large transmembrane proteins. The cyt bc_1 complex is a large multi-subunit complex, is very amphiphilic, having both significant soluble and membrane embedded domains, is molecularly complex, containing several non-proteinaceous cofactors, and has significant conformational dynamics within each domain of solubility during catalysis. Specifically, the cyt bc_1 complex from Rcaps contains three TM subunits per monomer of the natively homodimeric protein complex. The three subunits (cyt *b*, FeS, and cyt c_1) comprising each monomer contain a total of eight α-helical segments spanning the lipid phase,[28] constituting roughly 45% of the total protein backbone. Detergent solubilized purified cyt bc_1 complex samples also have three iron-containing cofactors in the form of two *b*- and one *c*-type hemes per monomer as well as a "Rieske"-type [2Fe−2S] cluster. Depending upon the extent and stringency of the purification process from Rcaps, various stoichiometries of ubiquinone, bacteriochlorophyll, native lipids,[29] and the detergent β-dodecylmaltoside will also be present. From a catalytic perspective, the cyt bc_1 complex carries out the reduction of two soluble electron carriers (cyt *c*) and one lipophilic carrier (ubiquinone) with reducing equivalents derived from the oxidation of two hydroquinone molecules via a modified and well-studied Q-cycle mechanism.[30−33] The catalysis involves a large-scale domain motion of the FeS subunit soluble domain[34−36] as well as conformational changes in the TM portion of the protein.[37−39] Here we present our findings that analysis of TM proteins is not only feasible by DUVRR but that this technique may represent a novel methodology for the analysis of membrane protein structure in the future.

■ MATERIALS AND METHODS

Cyt bc_1 Purification. Rcaps (pMTS1/MT-RBC1) was grown semiaerobically in the dark at 35 °C in MPYE medium supplemented with 10 μg mL^{-1} kanamycin as described previously.[40] Cells were stored at −80 °C until such time that chromatophore membranes were prepared and cyt bc_1 was isolated according to Valkova-Valchanova et al.[24] with the exception that DEAE−sepharose was used for the final anion exchange chromatography step. Cyt *c* and *b* content were verified by redox difference spectroscopy as described previously.[41] A 10 mg mL^{-1} stock was aliquoted and stored at −80 °C for DUVRR analysis.

DUVRR Spectroscopy. The DUVRR instrument is similar to those described previously.[42] Briefly, the fourth harmonic of a tunable Ti:sapphire laser (with excitation wavelengths ranging from 197 to 206 nm) was directed onto a thin film of sample flowing between two nitinol wires spaced about 1 mm apart under N_2 gas. Incident laser power at the sample was kept below 500 μW to minimize photodegradation; spectra were also monitored for photodegradation over time. Spectral calibration was carried out using a standard cyclohexane spectrum.[43] Cyt *c* from horse heart (Sigma) and cyt bc_1 solutions were prepared to 0.5 mg mL^{-1} in 20 and 120 mM phosphate buffer, respectively, containing the internal standard sodium perchlorate (50 and 100 mM, respectively).

Data Analysis. All DUVRR spectral preprocessing was carried out in a MATLAB environment using in house cosmic spike removal and water band removal methods described previously.[44] A nonlinear least-squares algorithm was carried out by fitting a mixture of Gaussian/Lorentzian peaks to experimental spectra as described previously.[45] Raman cross sections were calculated on a per amino acid residue basis based upon fitted peak intensities (eq 1).

$$\sigma_{\lambda,\,amide} = \frac{\sigma_{ClO_4^-}}{n}\,\frac{I_{amide}}{I_{ClO_4^-}}\left(\frac{\nu_{exc}-\nu_{ClO_4^-}}{\nu_{exc}-\nu_{amide}}\right)^4 \frac{C_{ClO_4^-}}{C_{amide}}\left(\frac{A_0 + A_{amide}}{A_0 + A_{ClO_4^-}}\right) \qquad (1)$$

At a given excitation wavelength, the absolute Raman cross section (in mbarn residue^{-1} steradian^{-1}), σ_{amide}, is derived from $\sigma_{ClO_4^-}$, the absolute Raman perchlorate cross section (mbarn molecule^{-1} steradian^{-1}),[42] where n is the number of residues in the peptide backbone, I is the Raman intensity (peak height) of perchlorate and amide mode, respectively, ν_{exc} is the excitation frequency (cm^{-1}), ν is the Raman shift of perchlorate and the amide mode (Δcm^{-1}), C is concentration (on a molar basis), and A is the UV absorbance of the sample at the excitation wavelength, A_0, the amide-shifted wavelength, A_{amide}, and the perchlorate-shifted wavelength, $A_{ClO_4^-}$.

■ RESULTS

DUVRR of Membrane and Soluble Proteins with Similar Overall Secondary Structural Content. In order to understand the contribution of the lipid environment of the peptide backbone to DUVRR spectra, two proteins with similar secondary structure and aromatic contents, horse heart cyt *c* and the TM protein cyt bc_1 complex (Figure 1, upper panel), were analyzed. DUVRR spectra were collected of samples containing 0.5 mg mL^{-1} of either cyt *c* or detergent (β-dodecylmaltoside, β-DM, 1:1 w/w) solubilized cyt bc_1 complex in phosphate buffer (pH 7.0) using an excitation wavelength of 197 nm. Despite the large difference in molecular size, total cofactor content, and the presence or absence of lipid, the DUVRR spectra for cyt *c* and the cyt bc_1 complex (Figure 1) were similar. Both spectra are dominated by intense features at 1001, 1206, 1266, and 1620 cm^{-1}, which can be assigned to

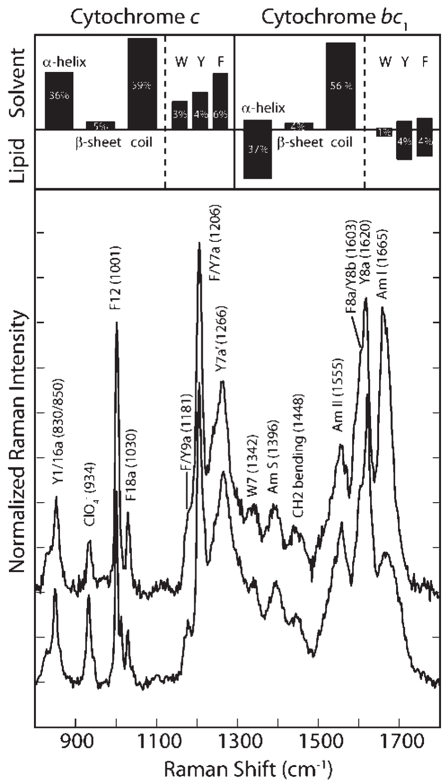

Figure 1. DUVRR spectra of aqueous and detergent solubilized proteins with similar secondary structure contents. DUVRR spectra of cyt *c* (lower spectrum) and cyt bc_1 (upper spectrum) excited at 197 nm are shown with vibrational mode assignments, and measured Raman shifts are also indicated for clarity. Spectra were normalized according to the internal standard ClO_4^- intensity and protein concentration. Total secondary structure and aromatic content derived from analysis of the Rcaps structural coordinates (PDB ID: 1ZRT) are shown in the upper panel.

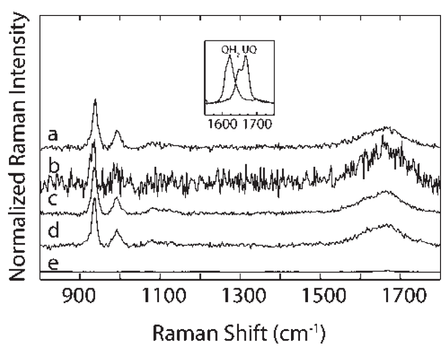

Figure 2. DUVRR spectra (λ_{ex} = 198 nm) of non-protein components in detergent solubilized cyt bc_1 complex samples. Spectra of a typical sample buffer (100 mM ClO_4^-, 120 mM phosphate (pH 7)) (a), excess bacteriochlorophyll in buffer (12 μM) (b), buffer with 0.5 mg mL^{-1} β-dodecylmaltoside (c), and 2.4 μM QH_2 with β-dodecylmaltoside (d), and with stoichiometric UQ in ethanol (e). Inset: DUVRR spectrum of 2.4 mM QH_2 in sample buffer and 0.75 mM UQ in ethanol.

contributions from the aromatic amino acid side chains, tyrosine and phenylalanine (Figure 1). Peptide backbone amide modes are also clearly visible at 1396 cm^{-1} (amide S), 1555 cm^{-1} (amide II), and 1665 cm^{-1} (amide I). The largest significant difference

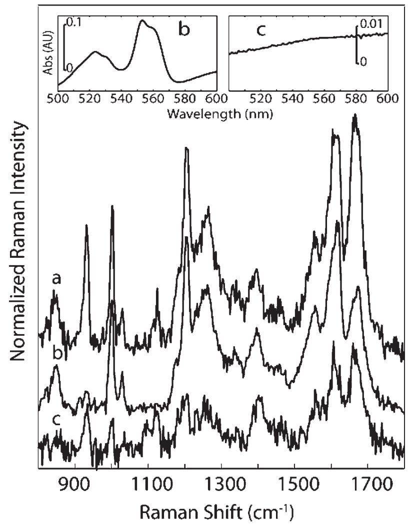

Figure 3. DUVRR spectra (λ_{ex} = 198 nm) of UQ diminished samples. DUVRR spectra of ascorbate-reduced cyt bc_1 at pH9 (a), the holocomplex subfractionation products the cyt *bc* subcomplex (b), and the Rieske Fe−S cluster (c). Corresponding dithionite-reduced minus ferricyanide-oxidized absorbance spectra of each subfraction sample (b) and (c) are displayed in the inset. DUVRR spectra are scaled for relative comparison of amide mode intensities.

between the two peptide DUVRR spectra is encountered in the amide I region corresponding to the carbonyl stretching mode. Specifically, the amide I mode in the cyt bc_1 complex sample appears to have a greater intensity vs the remaining amide modes as compared to the DUVRR spectra of the soluble cyt *c*.

To identify the molecular origin of the intense feature around 1670 cm^{-1} several non-proteinaceous molecules with carbonyl moieties were examined. DUVRR spectra of 0.5 mg mL^{-1} β-DM or methanol-solubilized bacteriochlorophyll (Bchl, 0.012 mM), two molecules known to be present in the cyt bc_1 complex preparations, showed no resonantly enhanced amide modes in the 1600−1700 cm^{-1} region of the spectrum (Figure 2). However, similar analysis of highly concentrated, 0.65 mg mL^{-1} (0.75 mM), ubiquinone-10 (UQ) in ethanol revealed a spectral feature at 1670 cm^{-1} similar to the feature seen in the cyt bc_1 complex DUVRR spectra (Figure 2, inset).

Despite the low concentrations of UQ expected to be present in the cyt bc_1 complex samples (∼<2 per monomer or <2 μM), two approaches were carried out to diminish the amount of oxidized quinone in a given sample, thereby determining its potential contribution to the cyt bc_1 complex DUVRR spectrum. The first approach involved diminishing the affinity of the protein sample for UQ by subfractionating the cyt bc_1 complex into the cyt *b* subunit, the cyt *bc* subcomplex, the single transmembrane domain containing FeS, and cyt c_1 subunits by size exclusion chromatography. Each of these subcomplexes will have little or no specific affinity for a UQ molecule. As expected, regardless of the subfraction analyzed, the intense amide I band remained in the DUVRR spectrum (Figure 3). Second, there were no differences between the oxidized and reduced DUVRR spectra of the holoenzyme in pH 9.0 phosphate buffer, where the UQ molecule bound at the higher affinity quinone reduction site (Q_i) in the cyt *b* subunit, should be converted to $QH^{\bullet-}$ or UQH_2.

dx.doi.org/10.1021/bi200596w | *Biochemistry* 2011, 50, 6531–6538

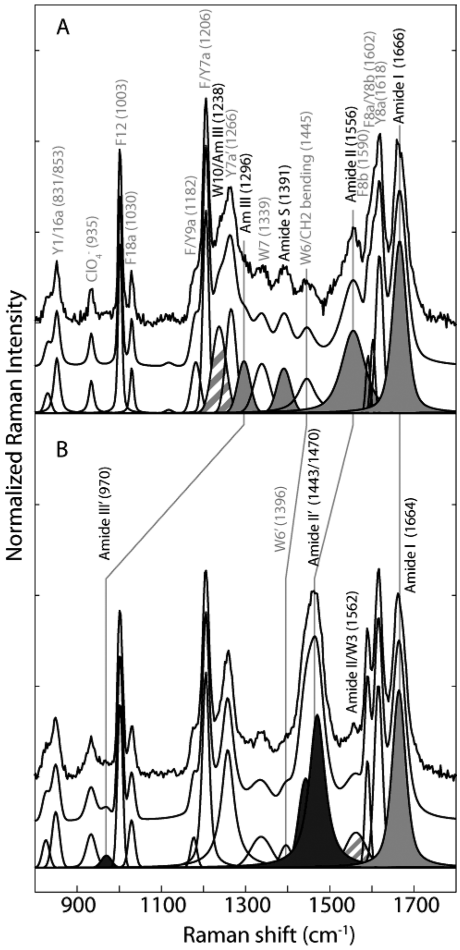

Figure 4. Effects of deuterium exchange on the cyt bc_1 complex DUVRR spectrum. Spectra (λ_{ex} = 197 nm) of cyt bc_1 in aqueous (panel A) and deuterated (panel B) buffer with raw spectra after baselining and buffer subtraction (top), a nonlinear least-squares fit (middle), and the individual fitted components (bottom) shown for comparative purposes. The Raman shifts of each assigned band are indicated for panel A and for panel B only if the band has shifted upon deuteration. Components correlative with amide modes are shaded in gray and labeled in black. All other bands are labeled in gray. In cases where amide and aromatic bands are fit by the same component, the fitted band is striped. Deuterated amide II′ and III′ modes are shaded a dark gray. The intensities of the spectra have been normalized as in Figure 1, and significant shifts due to deuteration are indicated by gray lines.

Identifying the H/D Exchangeable Portions of the Contributing Protein Spectra. The exclusion of detergent, cofactors, Bchl molecules, or quinones as the molecular cause of the intense 1665 cm^{-1} spectral feature prompted further studies into whether the increased amide I mode intensity could be derived from the TM (or region of limited solvent accessibility) portion of the protein backbone. DUVRR spectra (λ_{ex} = 197 nm) of cyt bc_1 complex samples were collected in aqueous phosphate buffer or buffer prepared with deuterium oxide. Immersion of the β-DM solvated cyt bc_1 complex in D_2O resulted in a diminished amide II feature at 1562 cm^{-1} coincident with the emergence of a new spectral feature at 1462 cm^{-1}, known to be the location of the N−D bend derived amide II′ mode (Figure 4). Much of the amide III mode contribution (1238/1296 cm^{-1}) also disappears from the spectrum, shifting to the amide III′ position (970 cm^{-1}) as documented previously,[46] which is also an indication of a significant influence of H^+/D^+ exchangeability over the DUVRR response. No significant differences in the amide I position or intensity were observed as a function of deuterium exchange, where the amide I mode would typically be expected to red shift and decrease slightly in intensity as a function of formation of the backbone N−D moiety upon exchange. A residual contribution to the DUVRR spectra at 1562 cm^{-1} can also be seen to remain despite exchange of the sample in D_2O for several days, indicating that at least some portion of the backbone was not solvent accessible.

Response of the Amide Modes to Excitation Wavelength. Despite the increased intensity of the 1665 cm^{-1} mode, other studies using UVRR of membrane proteins have not shown a similar spectral feature. However, all of these studies utilized excitation wavelengths >207 nm (predominantly >220 nm); therefore, we carried out studies to determine if the spectral response of this feature to excitation wavelength was only readily visible in the deep-UV. DUVRR spectra were collected of the cyt bc_1 complex at 197, 198, 200, 202, 204, and 206 nm (Figure 5, left panel). The enhancement of the 1665 cm^{-1} spectral feature more closely matches that of an aromatic residue than typical soluble protein amide I modes in both deuterium and non-deuterium exchanged spectra. While the amide I response to excitation energy was dramatically different between the soluble cyt c and the cyt bc_1 complex samples, the absolute Raman cross section of the amide II and amide S modes, normalized for the number of amino acid residues in each protein sample (eq 1), were virtually overlapped (Figure 5, middle panel). As expected, if the amide I mode was dominated by the nonexchanging TM region of the protein backbone, its DUVRR Raman cross-section excitation profile was very similar regardless of whether exchange was carried out (Figure 6, bottom panel). Additionally, consistent with a small portion of the amide I being derived from the >50% of the protein not embedded in the detergent micelle, the increase in the amide I response with increasing excitation energy is subtly diminished in the deuterium exchanged Raman cross-section excitation profile (Figure 6, top panel).

■ DISCUSSION

DUVRR Spectra of a Soluble and Partially Lipid-Solvated Protein. The overlapped DUVRR spectra of cyt c and cyt bc_1 complex are similar in all DUVRR spectral regions except for the amide I mode (Figure 1). The secondary structure and aromatic content similarities of the two protein samples led us to investigate whether the difference in the intensity of the amide I mode was derived from differences in the nonaqueous solvated peptide backbone content between the aqueous soluble cyt c and the surfactant micelle solubilized cyt bc_1 complex. DUVRR spectra of potential spectral contaminants associated with the purification of the cyt bc_1 complex from Rcaps confirmed that these molecules were not the source of the increased vibrational mode intensity at 1665 cm^{-1}. Lack of significant resonantly enhanced modes by these molecules is not surprising as porphyrin-containing cofactors, such as c-type cyt's or Bchl molecules, are not typically resonantly enhanced at excitation wavelengths near 197 nm. Therefore, the difference in the amide I mode between the two protein samples must be due to the protein itself and can be postulated to be related to

dx.doi.org/10.1021/bi200596w |Biochemistry 2011, 50, 6531–6538

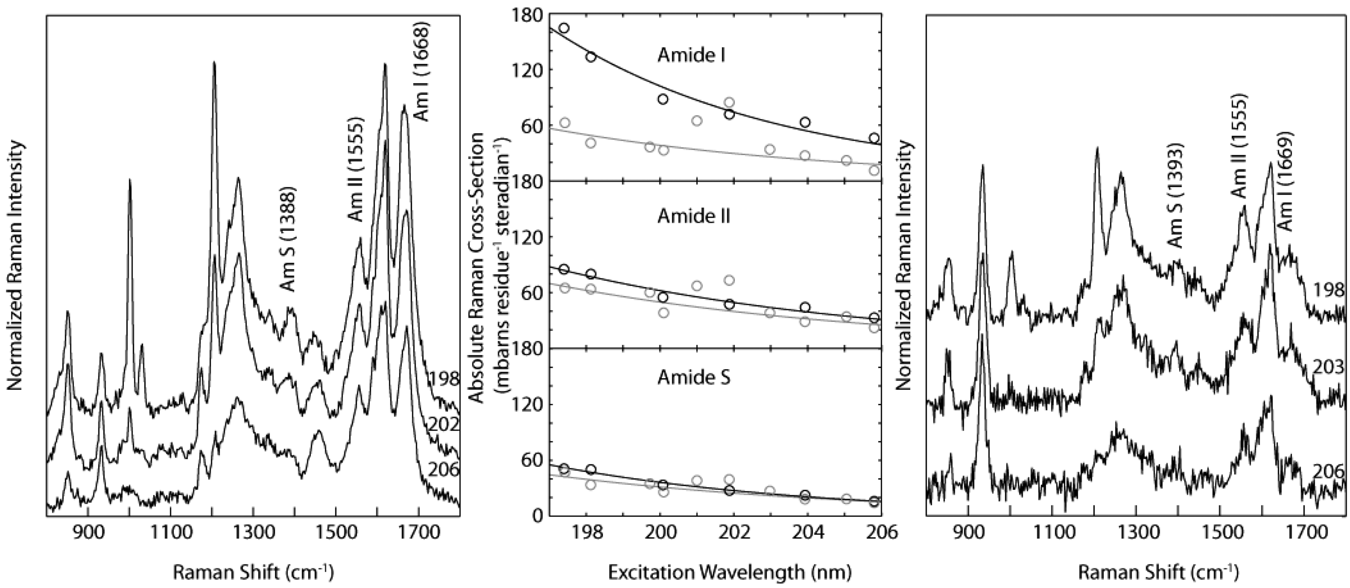

Figure 5. Excitation profiles of cyt bc_1 and cyt c. The absolute Raman cross sections (middle panel) were calculated based on intensities of the amide I, II, and S bands from 197 to 206 nm excitation. Black circles are calculated cross sections for cyt bc_1 spectra, and gray circles refer to cyt c spectra calculated cross sections. Only spectra of cyt bc_1 complex (left panel) and cyt c (right panel) collected at 198 nm (top), 202/203 nm (center), and 206 nm (bottom) excitation are shown for clarity; excitation wavelengths (nm) and amide assignments (with Raman shift in cm^{-1}) are indicated.

the solvent inaccessible TM domain of the cyt bc_1 complex (or its subfractions).

The peptide TM regions, or more specifically those embedded in the lipid or surfactant, are diminished with interaction of the solvent with the peptide backbone carbonyl and amines. Dehydration of the amide backbone has resulted previously in similar enhancements of the amide I mode.[15,47−49] Specifically, the DUVRR spectra of *n*-methylacetamide (NMA) in various solvents have been shown to exhibit changes in the intensities of all of the amide modes, including a very intense amide I compared the remaining amide modes in the more nonpolar solvents. Solvent-mediated hydrogen bonding perturbs the amide ground-state structure predominantly at the carbonyl compared to the adjacent amine, presumably because the C═O bond order is significantly altered by the electron-withdrawing hydrogen bonds (or their absence in less polar solvents).[15] Additional examples of loss of backbone hydration influencing the DUVRR spectrum of a protein backbone, and specifically the anticorrelated intensity changes of the amide I and II modes (increasing and decreasing in intensity, respectively) have also been observed with the depsipeptide valinomycin in various solvents[49] and in the interior cross β-sheet core of amyloid fibrils.[50,51] It remains unclear whether the solvent inaccessible regions of the α-helical TM regions of the cyt bc_1 complex exhibit similar diminished intensities of the amide II and III modes as NMA and valinomycin in nonpolar solvents.

The cyt bc_1 complex and its resulting DUVRR spectrum are mixtures of lipid-solvated and water-solvated domains. Previously, deuterium exchangeability had been used to delineate the DUVRR spectral signature of the solvent inaccessible interior (cross β-sheet core) from the solvated exterior of amyloid fibrils. Employing a similar strategy with the cyt bc_1 complex resulted in the expected decoupling of vibrational modes, eliminating most of the amide II, III, and S modes (Figure 4). However, assigning the remaining spectral feature at 1562 cm^{-1} to the amide II mode of the hydrophobic portion of the protein within a detergent micelle is not straightforward, as the peak position is also consistent with a tryptophan mode (W3), even though no other characteristic tryptophan modes are easily distinguished within the spectrum. The amide I, by contrast, is almost completely unaffected by deuteration, where classically, backbone deuteration would result in a small red shift and loss of intensity.[51,52] Lack of change in the amide I intensity and position as a function of H/D exchange implies that the bulk of the intensity of this mode is derived from the detergent-solvated region of the protein complex. Evidence of contribution of the exchangeable region of the protein to the amide I mode can be inferred from differences in the Raman cross sections between the pre- and post-deuterium-exchanged samples (Figure 6). Using the amide I cross sections of NMA at 200 nm excitation reported previously[15] in water and in acetonitrile, the water-solvated amide I can be estimated to be one-tenth of the area of the amide I from a lipid-solvated environment. Given that 45% of the backbone lies in the membrane, the difference in the aqueous and D_2O immersed cyt bc_1 samples indicate that roughly 10% of the total amide I mode intensity is derived from the water-solvated portion (∼55%) of the cyt bc_1 complex protein backbone or that the amide I mode response is 10 times more intense for the lipophilic portion of the protein backbone than its equivalent solvent-exposed portions. Lipid-solvated contributions to the amide III and S are not well resolved from the overlapped aromatics and cannot be compared with these analyses.

Lipid-Solvated α-Helical DUVRR Spectrum and Raman Cross Section. The excitation profile of all amide modes of NMA have been reported in both water and acetonitrile.[15,52] The nonpolar environment resulted in significant enhancement of the amide I mode compared to the amide II mode, a trend opposite to what is expected in water. This observation allows one to compare the amide I/amide II ratios as a means to probe the degree to which water has been excluded from the α-helical peptide backbone. The wavelength dependence of cyt bc_1 DUVRR spectra, for example, reveals a marked departure from cyt c (Figure 5). Most noticeably at 197 nm

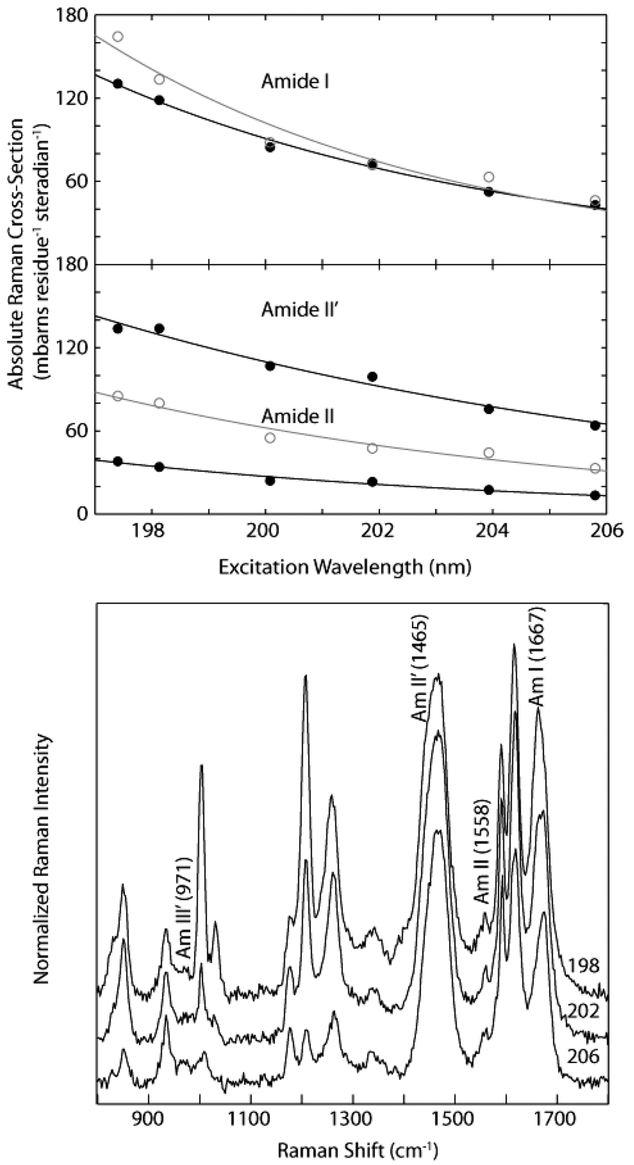

Figure 6. Excitation profile of cyt bc_1 in deuterated buffer. The absolute Raman cross sections of deuterated cyt bc_1 (black circles) were calculated based on band intensities from 197 to 206 nm excitation. Gray open circles indicate the absolute Raman cross sections of cyt bc_1 in aqueous buffer. Lines are included to guide the eye. Only spectra collected at 198 nm (top), 202 nm (center), and 206 nm (bottom) excitation are shown in the bottom panel for clarity; excitation wavelengths and amide assignments (with average associated Raman shift in cm^{-1}) are indicated.

excitation, the amide I is always more intense than the amide II. Excitation profiles of soluble proteins have been shown to be unique to specific secondary structure types.[45] The lipid-solvated region is entirely α-helical, and our es timation of the amide I intensity and position could serve as the basis for the first documented lipid-solvated α-helical UVRR spectrum. In addition to being much more intense, the maxima of the amide I mode is also significantly blue-shifted compared to those previously assigned to α-helical secondary structures in solvated protein and peptides. However, it remains unclear to what extent other factors, such as helical packing, might contribute to the amide I mode enhancement in this protein's DUVRR spectra compared to lipid-solubilized regions in other proteins.

A small number of previously published studies have used excitation wavelengths less than 210 nm to collect resonant Raman spectra of lipid or surfactant solvated proteins; however, none reported any remarkable feature associated with the amide I mode.[50,51,53−55] The clearest example can be seen in the works of Shafaat et al.[53] where the authors reported increased Raman cross sections for amide as well as tryptophan vibrational modes for a model β-strand hexapeptide consistent with the increased per residue amide I mode cross sections of cyt bc_1. The lack of a significant change in the Raman enhancement, especially of the amide I mode, reported in these studies using excitation wavelengths 207.5 nm, is consistent with excitation profiles of the cyt bc_1 complex presented here (Figure 5), where the amide I mode Raman cross section compared to the amide II mode decreases dramatically with decreasing excitation energies.

On the basis of previously assigned DUVRR amide signatures of aqueous solvated proteins and peptides,[12,13] the cyt bc_1 lipid-solvated region DUVRR spectral features described herein would have led to the erroneous assignment of the regions structure as a predominantly β-sheet or random coil dominated region of the protein merely as a function of its blue-shifted spectral position following H/D exchange experiments. However, it is clear from crystal structures the membrane-embedded TM portion of the protein is α-helical. Therefore, future efforts will need to concentrate on obtaining classical secondary structure signatures within the lipid phase before confident secondary structural content assignments can be made for membrane vs soluble domains of proteins using DUVRR.

■ CONCLUSION

Collection of resonance Raman spectra of lipid or surfactant solubilized proteins is feasible in the far deep-UV (<205 nm) despite the substantial absorbance of the sample at the excitation wavelengths used. The consequent resonant Raman enhancement of the peptide backbone associated with the desolvated regions of the protein have the potential to be a unique structural marker for membrane or lipid solvation of proteins and their structures. In fact, the ability of DUVRR spectroscopy to report on the peptide backbones solvation and structural constraints, while still gleaning site-specific information from naturally occurring aromatic residues make this technique a potentially valuable tool for analysis of the structural consequences of lipid−protein interactions.

■ ASSOCIATED CONTENT

S Supporting Information. CD spectrum of Rcaps cyt bc_1 (Figure 1). This material is available free of charge via the Internet at http://pubs.acs.org.

■ AUTHOR INFORMATION

Corresponding Author

*Phone: (573) 884-7525; fax: (573) 882-2754; e-mail: cooleyjw@missouri.edu.

Funding Sources

Funding was provided by the University of Missouri.

■ ABBREVIATIONS

Cytochrome bc_1, ubihydroquinone:cytochrome *c* oxidoreductase; DUVRR, deep ultraviolet resonance Raman; Rcaps, *Rhodobacter capsulatus*; TM, transmembrane; NMR, nuclear magnetic resonance; cyt, cytochrome; Fe−S, iron−sulfur; MPYE, mineral peptone yeast extract; β-DM, β-dodecylmaltoside; DEAE, diethylaminoethyl; BChl, bacteriochlorophyll; UQ, ubiquinone; NMA, *n*-methylacetamide; λ_{ex}, excitation wavelength.

■ REFERENCES

(1) White, S. H. (2004) The progress of membrane protein structure determination. *Protein Sci. 13*, 1948–1949.

(2) Arora, A., and Tamm, L. K. (2001) Biophysical approaches to membrane protein structure determination. *Curr. Opin. Struct. Biol. 11*, 540–547.

(3) Putnam, C. D., Hammel, M., Hura, G. L., and Tainer, J. A. (2007) X-ray solution scattering (SAXS) combined with crystallography and computation: defining accurate macromolecular structures, conformations and assemblies in solution. *Q. Rev. Biophys. 40*, 191–285.

(4) Han, X., Mihailescu, M., and Hristova, K. (2006) Neutron diffraction studies of fluid bilayers with transmembrane proteins: structural consequences of the achondroplasia mutation. *Biophys. J. 91*, 3736–3747.

(5) Skar-Gislinge, N., Simonsen, J. B., Mortensen, K., Feidenhans'l, R., Sligar, S. G., Møller, B. L., Bjørnholm, T., and Arleth, L. (2010) Elliptical structure of phospholipid bilayer nanodiscs encapsulated by scaffold proteins: casting the roles of the lipids and the protein. *J. Am. Chem. Soc. 132*, 13713–13722.

(6) Arrondo, J. L. R., and Goñi, F. M. (1999) Structure and dynamics of membrane proteins as studied by infrared spectroscopy. *Prog. Biophys. Mol. Biol. 72*, 367–405.

(7) Wallace, B. A. (2009) Protein characterisation by synchrotron radiation circular dichroism spectroscopy. *Q. Rev. Biophys. 42*, 317–370.

(8) Wallace, B. A., Lees, J. G., Orry, A. J. W., Lobley, A., and Janes, R. W. (2003) Analyses of circular dichroism spectra of membrane proteins. *Protein Sci. 12*, 875–884.

(9) Kim, J. E., Arjara, G., Richards, J. H., Gray, H. B., and Winkler, J. R. (2006) Probing folded and unfolded states of outer membrane protein A with steady-state and time-resolved tryptophan fluorescence. *J. Phys. Chem. B 110*, 17656–17662.

(10) Joo, C., Balci, H., Ishitzuka, Y., Buranachai, C., and Ha, T. (2008) Advances in single molecule fluorescence methods for molecular biology. *Annu. Rev. Biochem. 77*, 51–76.

(11) Matos, P. M., Franquelim, H. G., Castanho, M. A. R. B., and Santos, N. C. (2010) Quantitative assessment of peptide-lipid interactions. Ubiquitous fluorescence methodologies. *Biochim. Biophys. Acta 1798*, 1999–2012.

(12) Chi, Z., Chen, X. G., Holtz, J. S. W., and Asher, S. A. (1998) UV resonance Raman-selective amide vibrational enhancement: quantitative methodology for determining protein secondary structure. *Biochemistry 37*, 2854–2864.

(13) Huang, C.-Y., Balakrishnan, G., and Spiro, T. G. (2006) Protein secondary structure from deep-UV resonance Raman spectroscopy. *J. Raman Spectrosc. 37*, 277–282.

(14) Shashilov, V., Sikirzhytski, V., Popova, L. A., and Lednev, I. K. (2010) Quantitative methods for structural characterization of proteins based on deep UV resonance Raman spectroscopy. *Methods (Amsterdam, Neth.) 52*, 23–37.

(15) Wang, Y., Purrello, R., Georgiou, S., and Spiro, T. G. (1991) UVRR spectroscopy of the peptide bond. 2. Carbonyl H-bond effects on the ground- and excited-state structures of N-methylacetamide. *J. Am. Chem. Soc. 113*, 6368–6377.

(16) Triggs, N. E., and Valentini, J. J. (1992) An investigation of hydrogen bonding in amides using Raman spectroscopy. *J. Phys. Chem. 96*, 6922–6931.

(17) Mikhonin, A. V., Bykov, S. V., Myshakina, N. S., and Asher, S. A. (2006) Peptide secondary structure folding reaction coordinate: correlation between UV Raman amide III frequency, Ψ Ramachandran angle, and hydrogen bonding. *J. Phys. Chem. B 110*, 1928–1943.

(18) Myshakina, N. S., Ahmed, Z., and Asher, S. A. (2008) Dependence of amide vibrations on hydrogen bonding. *J. Phys. Chem. B 112*, 11873–11877.

(19) Huang, C.-Y., Balakrishnan, G., and Spiro, T. G. (2005) Early events in apomyoglobin unfolding probed by laser T-jump/UV resonance Raman spectroscopy. *Biochemistry 44*, 15734–15742.

(20) Asher, S. A., Ianoul, A., Mix, G., Boyden, M. N., Karnoup, A., Diem, M., and Schweitzer-Stenner, R. (2001) Dihedral ψ angle dependence of the amide III vibration: a uniquely sensitive UV resonance Raman secondary structural probe. *J. Am. Chem. Soc. 123*, 11775–11781.

(21) Chen, J., and Barry, B. A. (2008) Ultraviolet resonance Raman microprobe spectroscopy of photosystem II. *Photochem. Photobiol. 84*, 815–818.

(22) Chen, J., Bender, S. L., Keough, J. M., and Barry, B. A. (2009) Tryptophan as a probe of photosystem I electron transfer reactions: a UV resonance Raman study. *J. Phys. Chem. B 113*, 11367–11370.

(23) Sanchez, K. M., Neary, T. J., and Kim, J. E. (2008) Ultraviolet resonance Raman spectroscopy of folded and unfolded states of an integral membrane protein. *J. Phys. Chem. B 112*, 9507–9511.

(24) Valkova-Valchanova, M. B., Saribas, A. S., Gibney, B. R., Dutton, P. L., and Daldal, F. (1998) Isolation and characterization of a two-subunit cytochrome b-c_1 subcomplex from *Rhodobacter capsulatus* and reconstitution of its ubihydroquinone oxidation (Q_o) site with purified Fe-S protein subunit. *Biochemistry 37*, 16242–16251.

(25) Hunte, C., Palsdottir, H., and Trumpower, B. L. (2003) Protonmotive pathways and mechanisms in the cytochrome bc_1 complex. *FEBS Lett. 545*, 39–46.

(26) Xia, D., Yu, C.-A., Kim, H., Xia, J.-Z., Kachurin, A. M., Zhang, L., Yu, L., and Deisenhofer, J. (1997) Crystal structure of the cytochrome bc_1 complex from bovine heart mitochondria. *Science 277*, 60–66.

(27) Berry, E. A., Guergova-Kuras, M., Huang, L.-s., and Crofts, A. R. (2000) Structure and function of cytochrome *bc* complexes. *Annu. Rev. Biochem. 69*, 1005–1075.

(28) Berry, E. A., Huang, L.-s., Saechao, L. K., Pon, N. G., Valkova-Valchanova, M. B., and Daldal, F. (2004) X-ray structure of *Rhodobacter capsulatus* cytochrome bc_1: comparison with its mitochondrial and chloroplast counterparts. *Photosynth. Res. 81*, 251–275.

(29) Lange, C., Nett, J. H., Trumpower, B. L., and Hunte, C. (2001) Specific roles of protein-phospholipid interactions in the yeast cytochrome bc_1 complex structure. *EMBO J. 20*, 6591–6600.

(30) Crofts, A. R. (1985) The mechanism of the ubiquinol:cytochrome *c* oxidoreductases of mitochondria and of *Rhodopseudomonas sphaeroides*, in *The Enzymes of Biological Membranes* (Martonosi, A. N., Ed.) pp 347−382, Plenum Publ. Corp., New York.

(31) Trumpower, B. L., and Gennis, R. B. (1994) Energy transduction by cytochrome complexes in mitochondrial and bacterial respiration: the enzymology of coupling electron transfer reactions to transmembrane proton translocation. *Annu. Rev. Biochem. 63*, 675–716.

(32) Darrouzet, E., Cooley, J. W., and Daldal, F. (2004) The cytochrome bc_1 complex and its homologue the b_6f complex: similarities and differences. *Photosynth. Res. 79*, 25–44.

(33) Kramer, D. M., Nitschke, W., and Cooley, J. W. (2009) The Cytochrome bc_1 and Related *bc* Complexes: The Rieske/Cytochrome *b* Complex as the Functional Core of a Central Electron/Proton Transfer Complex, in *The Purple Phototrophic Bacteria* (Hunter, C. N., Daldal, F., Thurnauer, M. C., and Beatty, J. T., Eds.) pp 451−473, Springer, New York.

(34) Darrouzet, E., Valkova-Valchanova, M. B., Moser, C. C., Dutton, P. L., and Daldal, F. (2000) Uncovering the [2Fe2S] domain movement in cytochrome bc_1 and its implications for energy conversion. *Proc. Natl. Acad. Sci. U. S. A. 97*, 4567–4572.

(35) Xiao, K., Yu, L., and Yu, C.-A. (2000) Confirmation of the involvement of protein domain movement during the catalytic cycle of the cytochrome bc_1 complex by the formation of and intersubunit

disulfide bond between cytochrome *b* and the iron-sulfur protein. *J. Biol. Chem. 275*, 38597–38604.

(36) Darrouzet, E., and Daldal, F. (2002) Movement of the iron-sulfur subunit beyond the *ef* loop of cytochrome *b* is required for multiple turnovers of the bc_1 complex but not for single turnover Q_o site catalysis. *J. Biol. Chem. 277*, 3471–3476.

(37) Cooley, J. W., Ohnishi, T., and Daldal, F. (2005) Binding dynamics at the quinone reduction (Q_i) site influence the equilibrium interactions of the iron sulfur protein and hydroquinone oxidation (Q_o) site of the cytochrome bc_1 complex. *Biochemistry 44*, 10520–10532.

(38) Cooley, J. W., Lee, D.-W., and Daldal, F. (2009) Across membrane communication between the Q_o and Q_i active sites of cytochrome bc_1. *Biochemistry 48*, 1888–1899.

(39) Cooley, J. W. (2010) A structural model for across membrane coupling between the Q_o and Q_i active sites of cytochrome bc_1. *Biochim. Biophys. Acta 1797*, 1842–1848.

(40) Gray, K. A., Dutton, P. L., and Daldal, F. (1994) Requirement of histidine 217 for ubiquinone reductase activity (Q_i site) in the cytochrome bc_1 complex. *Biochemistry 33*, 723–733.

(41) van Gelder, B. F. (1978) Optical properties of cytochromes from beef heart mitochondria, submitochondrial vesicles, and derived preparations. *Methods Enzymol. 53*, 125–128.

(42) Balakrishnan, G., Hu, Y., Nielsen, S. B., and Spiro, T. G. (2005) Tunable kHz deep ultraviolet (193-210 nm) laser for Raman applications. *Appl. Spectrosc. 59*, 776–781.

(43) Ferraro, J. R., and Nakamoto, K. (1994) *Introductory Raman Spectroscopy*, Academic Press, Boston.

(44) Simpson, J. V., Oshokoya, O., Wagner, N., Liu, J., and JiJi, R. D. (2011) Pre-processing of ultraviolet resonance Raman spectra. *Analyst (Cambridge, U.K.) 136*, 1239–1247.

(45) Simpson, J. V., Balakrishnan, G., and JiJi, R. D. (2009) MCR-ALS analysis of two-way UV resonance Raman spectra to resolve discrete protein secondary structural motifs. *Analyst (Cambridge, U.K.) 134*, 138–147.

(46) Sugawara, Y., Kirakawa, A. Y., and Tsuboi, M. (1984) In-plane force constants of the peptide group: Least squares adjustment starting from *ab initio* values of *N*-methylacetamide. *J. Mol. Spectrosc. 108*, 206–214.

(47) Torii, H., Tatsumi, T., and Tasumi, M. (1998) Effects of hydration on the structure, vibrational wavenumbers, vibrational force field and resonance Raman intensities of *N*-methylacetamide. *J. Raman Spectrosc. 29*, 537–546.

(48) Markham, L. M., and Hudson, B. S. (1996) *Ab initio* analysis of the effects of aqueous solvation on the resonance Raman intensities of *N*-methylacetamide. *J. Phys. Chem. 100*, 2731–2737.

(49) Ozdemir, A., Lednev, I. K., and Asher, S. A. (2005) UVRR spectroscopic studies of valinomycin complex formation in different solvents. *Spectrochim. Acta, Part A 61*, 19–26.

(50) Xu, M., Shashilov, V., and Lednev, I. K. (2007) Probing the cross-β core structure of amyloid fibrils by hydrogen-deuterium exchange deep ultraviolet resonance Raman spectroscopy. *J. Am. Chem. Soc. 129*, 11002–11003.

(51) Popova, L. A., Kodali, R., Wetzel, R., and Lednev, I. K. (2010) Structural variations in the cross-β core of amyloid β fibrils revealed by deep UV resonance Raman spectroscopy. *J. Am. Chem. Soc. 132*, 6324–6328.

(52) Chen, X. G., Asher, S. A., Schweitzer-Stenner, R., Mirkin, N. G., and Krimm, S. (1995) UV Raman determination of the $\pi\pi^*$ excited state geometry of *N*-methylacetamide: vibrational enhancement pattern. *J. Am. Chem. Soc. 117*, 2884–2895.

(53) Shafaat, H. S., Sanchez, K. M., Neary, T. J., and Kim, J. E. (2009) Ultraviolet resonance Raman spectroscopy of a β-sheet peptide: a model for membrane protein folding. *J. Raman Spectrosc. 40*, 1060–1064.

(54) Cho, N., and Asher, S. A. (1996) UV resonance Raman and absorption studies of angiotensin II conformation in lipid environments. *Biospectroscopy 2*, 71–82.

(55) Holtz, J. S. W., Lednev, I. K., and Asher, S. A. (2000) UV resonance Raman study of angiotensin II conformation in nonaqueous environments: lipid micelles and acetonitrile. *Biopolymers 57*, 55–63.